Lecture Notes in Mechanical Engineering

Nguyen Tien Khiem
Tran Van Lien
Nguyen Xuan Hung *Editors*

Modern Mechanics and Applications

Select Proceedings of ICOMMA 2020

Springer

Lecture Notes in Mechanical Engineering

Series Editors

Francisco Cavas-Martínez, Departamento de Estructuras, Universidad Politécnica de Cartagena, Cartagena, Murcia, Spain

Fakher Chaari, National School of Engineers, University of Sfax, Sfax, Tunisia

Francesco Gherardini, Dipartimento di Ingegneria, Università di Modena e Reggio Emilia, Modena, Italy

Mohamed Haddar, National School of Engineers of Sfax (ENIS), Sfax, Tunisia

Vitalii Ivanov, Department of Manufacturing Engineering Machine and Tools, Sumy State University, Sumy, Ukraine

Young W. Kwon, Department of Manufacturing Engineering and Aerospace Engineering, Graduate School of Engineering and Applied Science, Monterey, CA, USA

Justyna Trojanowska, Poznan University of Technology, Poznan, Poland

Francesca di Mare, Institute of Energy Technology, Ruhr-Universität Bochum, Bochum, Nordrhein-Westfalen, Germany

Lecture Notes in Mechanical Engineering (LNME) publishes the latest developments in Mechanical Engineering—quickly, informally and with high quality. Original research reported in proceedings and post-proceedings represents the core of LNME. Volumes published in LNME embrace all aspects, subfields and new challenges of mechanical engineering. Topics in the series include:

- Engineering Design
- Machinery and Machine Elements
- Mechanical Structures and Stress Analysis
- Automotive Engineering
- Engine Technology
- Aerospace Technology and Astronautics
- Nanotechnology and Microengineering
- Control, Robotics, Mechatronics
- MEMS
- Theoretical and Applied Mechanics
- Dynamical Systems, Control
- Fluid Mechanics
- Engineering Thermodynamics, Heat and Mass Transfer
- Manufacturing
- Precision Engineering, Instrumentation, Measurement
- Materials Engineering
- Tribology and Surface Technology

To submit a proposal or request further information, please contact the Springer Editor of your location:

China: Ms. Ella Zhang at ella.zhang@springer.com
India: Priya Vyas at priya.vyas@springer.com
Rest of Asia, Australia, New Zealand: Swati Meherishi at swati.meherishi@springer.com
All other countries: Dr. Leontina Di Cecco at Leontina.dicecco@springer.com

To submit a proposal for a monograph, please check our Springer Tracts in Mechanical Engineering at http://www.springer.com/series/11693 or contact Leontina.dicecco@springer.com

Indexed by SCOPUS. All books published in the series are submitted for consideration in Web of Science.

More information about this series at http://www.springer.com/series/11236

Nguyen Tien Khiem · Tran Van Lien ·
Nguyen Xuan Hung
Editors

Modern Mechanics and Applications

Select Proceedings of ICOMMA 2020

Springer

Editors
Nguyen Tien Khiem
Vietnam Academy of Science and Technology
Hanoi, Vietnam

Tran Van Lien
National University of Civil Engineering
Hanoi, Vietnam

Nguyen Xuan Hung
Ho Chi Minh City University of Technology (HUTECH)
Ho Chi Minh, Vietnam

ISSN 2195-4356 ISSN 2195-4364 (electronic)
Lecture Notes in Mechanical Engineering
ISBN 978-981-16-3238-9 ISBN 978-981-16-3239-6 (eBook)
https://doi.org/10.1007/978-981-16-3239-6

© The Editor(s) (if applicable) and The Author(s), under exclusive license to Springer Nature Singapore Pte Ltd. 2022
This work is subject to copyright. All rights are solely and exclusively licensed by the Publisher, whether the whole or part of the material is concerned, specifically the rights of translation, reprinting, reuse of illustrations, recitation, broadcasting, reproduction on microfilms or in any other physical way, and transmission or information storage and retrieval, electronic adaptation, computer software, or by similar or dissimilar methodology now known or hereafter developed.
The use of general descriptive names, registered names, trademarks, service marks, etc. in this publication does not imply, even in the absence of a specific statement, that such names are exempt from the relevant protective laws and regulations and therefore free for general use.
The publisher, the authors and the editors are safe to assume that the advice and information in this book are believed to be true and accurate at the date of publication. Neither the publisher nor the authors or the editors give a warranty, expressed or implied, with respect to the material contained herein or for any errors or omissions that may have been made. The publisher remains neutral with regard to jurisdictional claims in published maps and institutional affiliations.

This Springer imprint is published by the registered company Springer Nature Singapore Pte Ltd.
The registered company address is: 152 Beach Road, #21-01/04 Gateway East, Singapore 189721, Singapore

Post-buckling Response of Functionally Graded Porous Plates Rested on Elastic Substrate via First-Order Shear Deformation Theory

Le Thanh Hai[1], Nguyen Van Long[2](✉), Tran Minh Tu[2], and Chu Thanh Binh[2]

[1] Faculty of Civil Engineering, Vinh University, Vinh, Vietnam
[2] Faculty of Industrial and Civil Engineering, National University of Civil Engineering, Hanoi, Vietnam
{longnv,tutm,binhct}@nuce.edu.vn

Abstract. This paper presents the post-buckling analysis of functionally graded porous (FGP) plates rested on the elastic substrate subjected to in-plane compressive mechanical loads. Based on the first-order shear deformation theory taking into account Von Karman nonlinearity, the governing equations are derived. The elastic modulus of FGP material is assumed to vary across the plate thickness following three various distribution patterns including uniform, symmetric, and asymmetric. Galerkin's approach and stress function is utilized to obtain the load-deflection relation for analyzing the post-buckling behavior of FGP plates. The theoretical formulation is verified by comparing the present results with those available in publications and found good agreement. Through the numerical results, the effect of porosity distribution pattern, porosity coefficient, geometrical configurations, elastic foundations, as well as mechanical loads on the post-buckling behavior of the FGP plate is indicated.

Keywords: Post-buckling · Porous plates · Analytical approach · First-order shear deformation theory · Stress function

1 Introduction

Functionally graded porous materials (FGPMs), such as metal foams, are ones of the category of lightweight materials and have potential applications in lightweight structures. Possesses many outstanding features such as excellent energy absorption capability, high specific strength, low thermal conductivity, etc., they are widely applied in aircraft, aerospace, ocean and civil engineering fields [1–3]. By adjusting the material composition, porosity patterns, pore size, and density the FGPMs can achieve the desire structural performance. Recently, the application of such materials tends to increase strongly, hence the studies on their mechanical behaviors have attracted considerable attention from scientist communities. Wattanasakulpong and Ungbhakorn [4] investigated the effect of porosities on the linear and nonlinear vibrational characteristic of FG beams under different types of elastic supports employing differential transformation method. Using Timoshenko beam theory and Ritz method, Chen et al. studied static and

© The Author(s), under exclusive license to Springer Nature Singapore Pte Ltd. 2022
N. Tien Khiem et al. (Eds.): *Modern Mechanics and Applications*, LNME, pp. 761–779, 2022.
https://doi.org/10.1007/978-981-16-3239-6_59

buckling behaviors [5], free and forced vibration [6], nonlinear free vibration [7] of FGP beams. Jabbari et al. presented buckling analysis [8] and thermal buckling analysis [9] of thin saturated FGP plates. Rezaei and Saidi [10] used Carrera unified formulation and state-space method to explore the effect of porosities on free vibrational characteristics of thick saturated FGP plates with Levy-type boundary conditions. Using simple first-order shear deformation theory (FSDT), Rezaei et al. [11] studied free vibration of FG plates with porosities by an analytical approach. Akbas [12] presented the effect of porosities on free vibration and bending behavior of FG plates by using Navier technique.

There are plenty researchers focusing on the post-buckling analysis of FG plates, i.e., Liew et al. [13] presented the post-buckling of FGM plates integrated with surface-bonded piezoelectric actuators subjected to in-plane force in the thermal environment applying the Galerkin-differential quadrature iteration algorithm; Bakora and Tounsi [14] studied post-buckling of thick FG plates subjected to thermomechanical loads; Feyzi and Khorshidvand [15] presented post-buckling of saturated porous circular plates subjected to mechanical load based on CLPT (classical plate theory); Tung and Duc [16] used classical plate theory and Galerkin's procedure to examine nonlinear stability of FG plates under thermo-mechanical loads; Cong et al. [17] investigated the effect of porosity distribution patterns on the thermomechanical buckling and post-buckling behavior of FG plate resting on elastic foundations; Barati and Zenkour [18] studied post-buckling of imperfect FG nanoplates with porosities by employing general higher-order plate theory and nonlocal elasticity; Using isogeometric analysis, Phung-Van et al. [19] investigated hygro-thermo-mechanical effects on the porosity-dependent geometrically nonlinear transient analysis of FGP plates based on third-order shear deformation theory.

In [20] Tu et al. examined the nonlinear buckling and post-buckling response FGP plates taking to account geometrical imperfect based on the CLPT. In this paper, we take a further step to analyze the post-buckling behavior of the FGP plates rested on Pasternak's foundation and subjected to uni-axial and bi-axial compressive loading. The theoretical formulation is developed by using the FSDT and von-Karman nonlinearity including the initial geometrical imperfection. The effective material properties of FGPMs (open-cell metal foam) are assumed to vary across the plate thickness according to a simple cosine rule. Three porosity distribution patterns such as uniform, non-uniform symmetric, non-uniform unsymmetric are considered. An analytical approach using stress function and Galerkin procedure is employed to obtain buckling loads, post-buckling load-deflection relation. The effects of material's properties, geometric parameters of the plates, elastic foundation stiffness on the post-buckling response of the plate are investigated through the numerical examples.

2 Functionally Graded Porous Plates

An FGP plate resting on Pasternak's elastic substrate with length a, width b and thickness h subjected to the bi-axial forces p_x, p_y is considered in this study. The coordinate system (x, y, z) is established in the middle plane as shown in Fig. 1. The Pasternak foundation with Winkler stiffness K_w, shear stiffness K_{si} $(i = x, y)$.

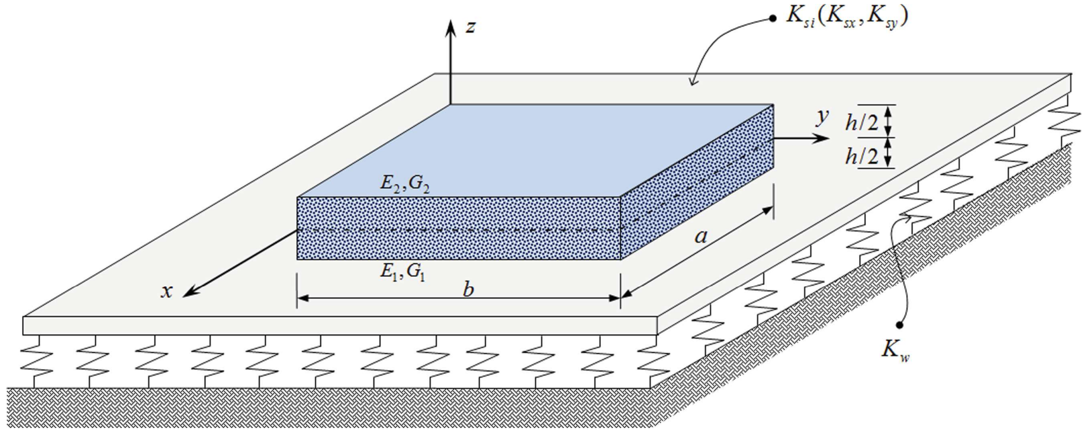

Fig. 1. Functionally graded porous plate on elastic foundation

The open-cell metal foam with three porosity distribution patterns along the thickness direction is considered (see Fig. 2). The elastic moduli of each pattern can be determined as follow [21, 22]

$$\text{Type 1: Uniform distribution: } \{E,G\} = \{E_1,G_1\}(1-e_0\lambda);\ \ \lambda = \frac{1}{e_0}\left[1-\left(\frac{2}{\pi}\sqrt{1-e_0}-\frac{2}{\pi}+1\right)^2\right] \quad (1)$$

$$\text{Type 2 : Non - uniform symmetric distribution:}\{E(z), G(z)\} = \{E_1, G_1\}\left[1 - e_0 \cos\left(\frac{\pi z}{h}\right)\right] \quad (2)$$

$$\text{Type 3 : Non - uniform asymmetric distribution : }\{E(z), G(z)\} = \{E_1, G_1\}\left[1 - e_0 \cos\left(\frac{\pi z}{2h} + \frac{\pi}{4}\right)\right] \quad (3)$$

in which: E_1, G_1, E_2, G_2 are maximum and minimum values of Young's modulus, shear modulus respectively. Poisson ratio is assumed to be constant.

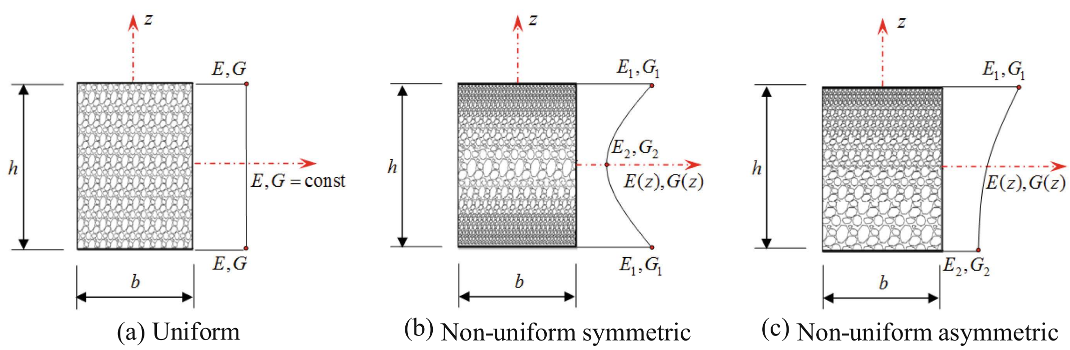

Fig. 2. The three types of porosity distribution

The porosity coefficient e_0 is defined as

$$e_0 = 1 - \frac{E_2}{E_1} = 1 - \frac{G_2}{G_1}; \quad (0 < e_0 < 1) \quad (4)$$

Herein, the physical neutral surface is chosen as the reference surface to vanish the stretching–bending coupling effect in constitutive equations. For the case of non-uniform asymmetric porosity distribution, the neutral surface position is defined as [23]:

$$\int_{-h/2}^{h/2} (z - C)E(z)dz = 0 \quad \Rightarrow C = \left[\int_{-h/2}^{h/2} zE(z)dz \right] / \left[\int_{-h/2}^{h/2} E(z)dz \right] \tag{5}$$

3 Theoretical Formulation

Using the physical neutral surface concept, the displacements $\tilde{u}$, $\tilde{v}$, $\tilde{w}$ according to FSDT in the coordinate system (x, y, z_{ns}) take the following form [24]:

$$\begin{aligned} &\tilde{u}(x, y, z_{ns}) = u_0(x, y) + z_{ns}\vartheta_x(x, y); \quad \tilde{v}(x, y, z_{ns}) = v_0(x, y) + z_{ns}\vartheta_y(x, y); \\ &\tilde{w}(x, y, z_{ns}) = w_0(x, y) \end{aligned} \tag{6}$$

where u_0, v_0, w_0 are displacements on the physical neutral surface along
the directions x, y, and z_{ns}, respectively; and ϑ_x, ϑ_y are neutral surface rotations of transverse normal about y-, x- axes respectively.

The nonzero strains at the neutral surface of the FGP plate, including von Kárman nonlinearity, and initial geometrical imperfection w_0^*, are given as follows [24]:

$$\begin{Bmatrix} \varepsilon_x \\ \varepsilon_y \\ \gamma_{xy} \end{Bmatrix} = \begin{Bmatrix} \varepsilon_x^0 \\ \varepsilon_y^0 \\ \gamma_{xy}^0 \end{Bmatrix} + z_{ns} \begin{Bmatrix} k_x \\ k_y \\ k_{xy} \end{Bmatrix}; \begin{Bmatrix} \gamma_{xz} \\ \gamma_{yz} \end{Bmatrix} = \begin{Bmatrix} \gamma_{xz}^0 \\ \gamma_{yz}^0 \end{Bmatrix} \tag{7}$$

in which: $\varepsilon_x^0 = u_{0,x} + \frac{w_{0,x}^2}{2} + w_{0,x}w_{0,x}^*$; $k_x = \theta_{x,x}$; $\varepsilon_y^0 = v_{0,y} + \frac{w_{0,y}^2}{2} + w_{0,y}w_{0,y}^*$; $k_y = \vartheta_{y,y}$; $\gamma_{xy}^0 = u_{0,y} + v_{0,x} + w_{0,x}w_{0,y} + w_{0,y}w_{0,x}^* + w_{0,x}w_{0,y}^*$; $k_{xy} = \vartheta_{x,y} + \vartheta_{y,x}$; $\gamma_{xz}^0 = w_{0,x} + \vartheta_x$; $\gamma_{yz}^0 = w_{0,y} + \vartheta_y$.

The comma followed by x or y denotes the differentiation with respect to the x or y coordinates respectively.

The stress-strain relationships for the FGP plate are given by:

$$\begin{Bmatrix} \sigma_x \\ \sigma_y \\ \sigma_{xy} \end{Bmatrix} = \begin{bmatrix} Q_{11} & Q_{12} & 0 \\ Q_{21} & Q_{22} & 0 \\ 0 & 0 & Q_{66} \end{bmatrix} \begin{Bmatrix} \varepsilon_x \\ \varepsilon_y \\ \gamma_{xy} \end{Bmatrix}; \begin{Bmatrix} \sigma_{xz} \\ \sigma_{yz} \end{Bmatrix} = \begin{bmatrix} Q_{55} & 0 \\ 0 & Q_{44} \end{bmatrix} \begin{Bmatrix} \gamma_{xz} \\ \gamma_{yz} \end{Bmatrix} \tag{8}$$

in which: $Q_{11} = Q_{22} = \frac{1}{1-\nu^2}E(z_{ns})$, $Q_{12} = Q_{21} = \frac{\nu}{1-\nu^2}E(z_{ns})$, $Q_{44} = Q_{55} = Q_{66} = \frac{1}{2(1+\nu)}E(z_{ns})$.

The constitutive relations of FGP plate based on the physical neutral surface concept are described as follow:

$$\begin{Bmatrix} N_x \\ N_y \\ N_{xy} \end{Bmatrix} = \begin{bmatrix} \tilde{A}_{11} & \tilde{A}_{12} & 0 \\ \tilde{A}_{12} & \tilde{A}_{11} & 0 \\ 0 & 0 & \tilde{A}_{66} \end{bmatrix} \begin{Bmatrix} \varepsilon_x^0 \\ \varepsilon_y^0 \\ \gamma_{xy}^0 \end{Bmatrix}; \begin{Bmatrix} M_x \\ M_y \\ M_{xy} \end{Bmatrix} = \begin{bmatrix} \tilde{C}_{11} & \tilde{C}_{12} & 0 \\ \tilde{C}_{12} & \tilde{C}_{11} & 0 \\ 0 & 0 & \tilde{C}_{66} \end{bmatrix} \begin{Bmatrix} k_x \\ k_y \\ k_{xy} \end{Bmatrix}; \quad (9)$$

$$\begin{Bmatrix} Q_{xz} \\ Q_{yz} \end{Bmatrix} = \begin{bmatrix} \tilde{A}_{44}^s & 0 \\ 0 & \tilde{A}_{44}^s \end{bmatrix} \begin{Bmatrix} \gamma_{xz}^0 \\ \gamma_{yz}^0 \end{Bmatrix}$$

where: $\tilde{A}_{ij} = \int\limits_{-h/2-C}^{h/2-C} Q_{ij} dz_{ns}$; $\tilde{C}_{ij} = \int\limits_{-h/2-C}^{h/2-C} Q_{ij} z_{ns}^2 dz_{ns}$; $\tilde{A}_{44}^s = k_s \int\limits_{-h/2-C}^{h/2-C} Q_{44} dz_{ns}$; $ij = 11, 12, 66$;

For metal foam, the shear correction factor $k_s = 5/6$ is used.

The equilibrium equations of FGP plate resting on the elastic foundation are derived from principle minimum total energy [25], its mathematical formulation has the form:

$$0 = \delta U_P + \delta U_F + \delta V \quad (10)$$

where δU_P, δU_F, δV are the variation of plate strain energy, of Pasternak's foundation strain energy, and work done by external loads, respectively.

The obtained equilibrium equations are expressed as [25]:

$$\partial N_x/\partial x + \partial N_{xy}/\partial y = 0; \quad (11.1)$$

$$\partial N_y/\partial y + \partial N_{xy}/\partial x = 0; \quad (11.2)$$

$$\begin{aligned} &\partial Q_{yz}/\partial y + \partial Q_{xz}/\partial x + N_x \partial^2 w_0/\partial x^2 + 2N_{xy}\partial^2 w_0/\partial x\partial y \\ &+ N_y \partial^2 w_0/\partial y^2 - K_w w_0 + K_{sx}\partial^2 w_0/\partial x^2 + K_{sy}\partial^2 w_0/\partial y^2 = 0; \end{aligned} \quad (11.3)$$

$$Q_{xz} - \partial M_x/\partial x - \partial M_{xy}/\partial y = 0; \quad (11.4)$$

$$Q_{yz} - \partial M_{xy}/\partial x - \partial M_y/\partial y = 0; \quad (11.5)$$

By introducing the stress functions as follow:

$$N_x = \partial^2\varphi/\partial y^2; \quad N_y = \partial^2\varphi/\partial x^2; \quad N_{xy} = -\partial^2\varphi/\partial x\partial y \quad (12)$$

Two Eqs. (11.1)–(11.2) are identically satisfied. Using the relations (7), (9) and (12), the system of equilibrium equations is rewritten in terms of displacements and stress function as follow

$$\begin{aligned} &\tilde{A}_{44}^s \partial^2 w_0/\partial y^2 + \tilde{A}_{44}^s \partial^2 w_0/\partial x^2 + \tilde{A}_{44}^s \partial\vartheta_x/\partial x + \tilde{A}_{44}^s \partial\vartheta_y/\partial y - K_w w_0 \\ &+ K_{sx}\partial^2 w_0/\partial x^2 + K_{sy}\partial^2 w_0/\partial y^2 + \partial\varphi/\partial y^2\left(\partial^2 w_0/\partial x^2 + \partial^2 w_0^*/\partial x^2\right) \\ &- 2\partial^2\varphi/\partial x\partial y\left(\partial^2 w_0/\partial x\partial y + \partial^2 w_0^*/\partial x\partial y\right) + \partial\varphi/\partial x^2\left(\partial^2 w_0/\partial y^2 + \partial^2 w_0^*/\partial y^2\right) = 0; \end{aligned} \quad (13.1)$$

$$\tilde{C}_{11}\partial^2\vartheta_x/\partial x^2 + \tilde{C}_{66}\partial^2\vartheta_x/\partial y^2 + \left(\tilde{C}_{12} + \tilde{C}_{66}\right)\partial^2\vartheta_y/\partial x\partial y - \tilde{A}^s_{44}\vartheta_x - \tilde{A}^s_{55}\partial w_0/\partial x = 0; \tag{13.2}$$

$$\left(\tilde{C}_{12} + \tilde{C}_{66}\right)\partial^2\vartheta_x/\partial x\partial y + \tilde{C}_{66}\partial^2\vartheta_y/\partial x^2 + \tilde{C}_{11}\partial^2\vartheta_y/\partial y^2 - \tilde{A}^s_{44}\vartheta_y - \tilde{A}^s_{44}\partial w_0/\partial y = 0 \tag{13.3}$$

The geometrical compatibility equation is written as [26]:

$$\begin{aligned}&\partial^2\varepsilon^0_x/\partial y^2 + \partial_2\varepsilon^0_y/\partial x^2 - \partial^2\gamma^0_{xy}/\partial x\partial y = \partial^2 w_0^2/\partial x\partial y - \partial^2 w_0/\partial x^2.\partial^2 w_0/\partial y^2\\&+2\partial^2 w_0/\partial x\partial y.\partial^2 w_0^*/\partial x\partial y - \partial^2 w_0/\partial x^2.\partial^2 w_0^*/\partial y^2 - \partial^2 w_0/\partial y^2.\partial^2 w_0^*/\partial x^2\end{aligned} \tag{14}$$

From Eqs. (9) and (12), the strains can be expressed as

$$\begin{aligned}\varepsilon^0_x &= \frac{\tilde{A}_{11}}{\tilde{A}^2_{11}-\tilde{A}^2_{12}}N_x - \frac{\tilde{A}_{12}}{\tilde{A}^2_{11}-\tilde{A}^2_{12}}N_y = \frac{\tilde{A}_{11}}{\tilde{A}^2_{11}-\widehat{A}^2_{12}}\frac{\partial^2\varphi}{\partial y^2} - \frac{\tilde{A}_{12}}{\widehat{A}^2_{11}-\tilde{A}^2_{12}}\frac{\partial^2\varphi}{\partial x^2};\\ \varepsilon^0_y &= \frac{\tilde{A}_{11}}{\tilde{A}^2_{11}-\tilde{A}^2_{12}}N_y - \frac{\tilde{A}_{12}}{\tilde{A}^2_{11}-\tilde{A}^2_{12}}N_x = \frac{\tilde{A}_{11}}{\widehat{A}^2_{11}-\tilde{A}^2_{12}}\frac{\partial^2\varphi}{\partial x^2} - \frac{\tilde{A}_{12}}{\tilde{A}^2_{11}-\tilde{A}^2_{12}}\frac{\partial^2\varphi}{\partial y^2};\ \gamma^0_{xy} = \frac{1}{A_{66}}N_{xy} = -\frac{1}{A_{66}}\varphi_{,xy}\end{aligned} \tag{15}$$

Substituting the Eq. (15) into geometrical compatibility Eq. (14), we obtain:

$$\begin{aligned}\nabla^4\varphi = D\Big(&\partial^2 w_0^2/\partial x\partial y - \partial^2 w_0/\partial x^2.\partial^2 w_0/\partial y^2 + 2w_0/\partial x\partial y.w_0^*/\partial x\partial y\\&- \partial^2 w_0/\partial x^2.\partial^2 w_0^*/\partial y^2 - \partial^2 w_0/\partial y^2.\partial^2 w_0^*/\partial x^2\Big)\end{aligned} \tag{16}$$

in which: $\nabla^4 = \frac{\partial^4}{\partial x^4} + 2\frac{\partial^4}{\partial x^2\partial y^2} + \frac{\partial^4}{\partial y^4}$; $D = \tilde{A}_{11}\left(1-\nu^2\right)$.

Four Eqs. (13.1)–(13.3) and (16) are nonlinear equations with four unknowns $w_0, \vartheta_x, \vartheta_y, \varphi$. and used to analyze the buckling and post-buckling response of FGP plates taking to account initial geometrical imperfection.

4 Buckling and Postbuckling Analysis

In this study, three types of boundary conditions (BCs.), referred to as four edges are simply supported and freely moveable (SSSS), four edges are clamped and freely moveable (CCCC), and two opposite edges are simply supported, the remaining edges are clamped and freely moveable (SCSC) are considered:

– SSSS with associated boundary conditions as

$$w_0 = \vartheta_s = 0;\ N_{ns} = 0; M_n = 0; N_n = N_{n0} \tag{17}$$

– CCCC with associated boundary conditions as

$$w_0 = \vartheta_n = \vartheta_s = 0;\ N_{ns} = 0; N_n = N_{n0} \tag{18}$$

– SCSC with associated boundary conditions as

$$\begin{array}{l} \text{at}\, x = 0, a : w_0 = \vartheta_y = 0;\; N_{xy} = 0; M_x = 0;\; N_x = N_{x0} \\ \text{at}\, y = 0, b : w_0 = \vartheta_x = \vartheta_y = 0;\; N_{xy} = 0; N_y = N_{y0} \end{array} \tag{19}$$

in which N_{x0}, N_{y0} are in-plane compressive loads at movable edges along the directions x, y, respectively.

a. ***Boundary conditions SSSS***

For this BC, the solutions are chosen as [16, 27, 28]:

$$\begin{array}{l} w_0 = w_{0mn} \sin\alpha x \sin\beta y;\; \vartheta_x = \vartheta_{xmn} \cos\alpha x \sin\beta y; \\ \vartheta_y = \vartheta_{ymn} \sin\alpha x \cos\beta y;\; w_0^* = \xi h \sin\alpha x \sin\beta y \end{array} \tag{20}$$

where: $\alpha = \frac{m\pi}{a},\ \beta = \frac{n\pi}{b};\ m, n$ are the number of half-waves in x and y directions; $w_{0mn}, \vartheta_{xmn},\ \vartheta_{ymn}$ are unknown coefficients to be determined; the coefficient $\xi \in [0, 1]$ represents an FGP plate imperfection size.

Putting Eq. (20) into Eq. (16), we obtain:

$$\nabla^4\varphi = \frac{D\left(w_{0mn}^2 + 2\xi h w_{0mn}\right)\alpha^2\beta^2}{2}(\cos 2\alpha x + \cos 2\beta y) \tag{21}$$

The stress function may be assumed in the following form:

$$\varphi = f_1 \cos 2\alpha x + f_2 \cos 2\beta y + N_{x0}\frac{y^2}{2} + N_{y0}\frac{x^2}{2} \tag{22}$$

where: $f_1 = \frac{D\beta^2}{32\alpha^2}\left(w_{0mn}^2 + 2\xi h w_{0mn}\right);\ f_2 = \frac{D\alpha^2}{32\beta^2}\left(w_{0mn}^2 + 2\xi h w_{0mn}\right)$.

Substituting the solutions (20) into two Eqs. (13.2) and (13.3), the rotations are determined as

$$\vartheta_{xmn\,xmn} = D_1 w_{0mn};\;\; \vartheta_{ymn} = D_2 w_{0mn} \tag{23}$$

in which: $D_1 = \frac{B_1C_2 - B_2C_1}{A_1B_2 - A_2B_1};\ D_2 = \frac{A_2C_1 - A_1C_2}{A_1B_2 - A_2B_1};\ A_1 = \tilde{C}_{11}\alpha^2 + \tilde{C}_{66}\beta^2 + \tilde{A}_{44}^s;\ A_2 = B_1 = \left(\tilde{C}_{12} + \tilde{C}_{66}\right)\alpha\beta;\ B_2 = \left(\tilde{C}_{66}\alpha^2 + \tilde{C}_{11}\beta^2 + \tilde{A}_{44}^s\right);\ C_1 = \tilde{A}_{44}^s\alpha;\ C_2 = \tilde{A}_{44}^s\beta.$

By substituting Eqs. (22) and (23) into Eq. (13.1) and then applying Galerkin's procedure, we get:

$$c_{1a}w_{0mn} + \left(N_{x0}\alpha^2 + N_{y0}\beta^2\right)(w_{0mn} + \xi h) + c_{2a}\left(w_{0mn}^2 + 2\xi h w_{0mn}\right)(w_{0mn} + \xi h) = 0. \tag{24}$$

where: $c_{1a} = \left(\tilde{A}_{44}^s + K_{sy}\right)\beta^2 + \left(\tilde{A}_{44}^s + K_{sx}\right)\alpha^2 + (D_1\alpha + D_2\beta)\tilde{A}_{44}^s + K_w;\ c_{2a} = \frac{(\alpha^4+\beta^4)D}{16}$.

Consider an FGP plate subjected to bi-axial compressive loads $N_x^0 = -\gamma_1 N_0 h$, $N_y^0 = -\gamma_2 N_0 h$ in the edges $x = 0,\ a$ and $y = 0,\ b$. From the Eq. (24) we have

$$N_0 = \frac{c_{1a}}{\gamma_1\alpha^2 + \gamma_2\beta^2}\frac{\bar{W}}{\left(\bar{W} + \xi\right)h} + \frac{c_{2a}}{\gamma_1\alpha^2 + \gamma_2\beta^2}\left(\bar{W}^2 + 2\xi\bar{W}\right)h; \quad \bar{W} = \frac{w_{0mn}}{h} \tag{25}$$

It is the basic equations used to study the nonlinear post-buckling behavior of perfect and imperfect FGP plate including the critical load determination and load-deflection curve investigation.

For perfect plates, $\xi = 0$; because $w_{0mn} \neq 0$, the compressive load is derived in the form:

$$N_0^* = \frac{c_{1a}}{\left(\gamma_1\alpha^2 + \gamma_2\beta^2\right)h} + \frac{c_{2a}}{\gamma_1\alpha^2 + \gamma_2\beta^2}\bar{W}^2 h \tag{26}$$

The buckling load obtained:

$$N_{bl} = \frac{c_{1a}}{\left(\gamma_1\alpha^2 + \gamma_2\beta^2\right)h} \tag{27}$$

The buckling loads N_{bl} expressed by Eq. (27) belong to corresponding buckling modes $(m,\ n)$. The critical buckling load N_{cr} is the minimal value of these buckling loads.

Thus, for perfect plates $\xi = 0$, the function N_0^* reaches the minimum at $w_{0mn} = 0$ and $N_{bl} = N_0^*\big|_{w_{0mn}=0}$.

b. ***Boundary conditions CCCC***

For this type of boundary condition, the solutions are chosen as [27, 28]:

$$\begin{gathered} w_0 = w_{0mn}\sin^2\alpha x\sin^2\beta y;\ \ \vartheta_x = \vartheta_{xmn}\sin 2\alpha x\sin^2\beta y \\ \vartheta_y = \vartheta_{ymn}\sin^2\alpha x\sin 2\beta y;\ \ w_0^* = \xi h\sin^2\alpha x\sin^2\beta y \end{gathered} \tag{28}$$

Substituting Eq. (28) into Eq. (16), we get:

$$\nabla^4\varphi = \frac{D\left(w_{0mn}^2 + 2\xi h w_{0mn}\right)\alpha^2\beta^2}{2}\begin{pmatrix} \cos 2\alpha x + \cos 2\beta y - \cos 4\alpha x - \cos 4\beta y \\ -2\cos 2\alpha x\cos 2\beta y + \cos 2\alpha x\cos 4\beta y + \cos 4\alpha x\cos 2\beta y \end{pmatrix} \tag{29}$$

The stress function may be assumed in the following form:

$$\begin{aligned} \varphi = {} & f_1\cos 2\alpha x + f_2\cos 2\beta y + f_3\cos 4\alpha x + f_4\cos 4\beta y + f_5\cos 2\alpha x\cos 2\beta y \\ & + f_6\cos 2\alpha x\cos 4\beta y + f_7\cos 4\alpha x\cos 2\beta y + N_{x0}\frac{y^2}{2} + N_{y0}\frac{x^2}{2} \end{aligned} \tag{30}$$

where: $f_1 = \frac{D\beta^2}{64\alpha^2}\left(w_{0mn}^2 + 2\xi h w_{0mn}\right)$; $f_2 = \frac{D\alpha^2}{64\beta^2}\left(w_{0mn}^2 + 2\xi h w_{0mn}\right)$; $f_3 = \frac{D\beta^2}{1024\alpha^2}\left(w_{0mn}^2 + 2\xi h w_{0mn}\right)$; $f_4 = \frac{D\alpha^2}{1024\beta^2}\left(w_{0mn}^2 + 2\xi h w_{0mn}\right)$;

$f_5 = \frac{Da^2\beta^2}{64(\alpha^2+\beta^2)^2}\left(w_{0mn}^2 + 2\xi h w_{0mn}\right)$; $f_6 = \frac{Da^2\beta^2}{64(\alpha^2+4\beta^2)^2}\left(w_{0mn}^2 + 2\xi h w_{0mn}\right)$; $f_7 = \frac{Da^2\beta^2}{64(4\alpha^2+\beta^2)^2}\left(w_{0mn}^2 + 2\xi h w_{0mn}\right)$.

Substituting Eq. (30) into Eqs. (13.2) and (13.3), applying Galerkin's procedure, we obtain rotations in term of deflections:

$$\vartheta_{xmn} = D_1 w_{0mn};\ \vartheta_{ymn} = D_2 w_{0mn}; \tag{31}$$

in which: $D_1 = \frac{B_1C_2 - B_2C_1}{A_1B_2 - A_2B_1}$; $D_2 = \frac{A_2C_1 - A_1C_2}{A_1B_2 - A_2B_1}$; $A_1 = 12\tilde{C}_{11}\alpha^2 + 4\tilde{C}_{66}\beta^2 + 3\tilde{A}_{55}^s$; $A_2 = 4\left(\tilde{C}_{66} + \tilde{C}_{21}\right)\alpha\beta$; $B_1 = 4\left(\tilde{C}_{12} + \tilde{C}_{66}\right)\alpha\beta$; $B_2 = \left(4\tilde{C}_{66}\alpha^2 + 12\tilde{C}_{22}\beta^2 + 3\tilde{A}_{44}^s\right)$; $C_1 = 3\tilde{A}_{55}^s\alpha$; $C_2 = 3\tilde{A}_{44}^s\beta$.

By substituting Eqs. (30) and (31) into Eq. (13.1) and then implementing Galerkin's procedure, leads to:

$$w_{0mn}c_{1b} + (w_{0mn} + \xi h)\left[N_{x0}\alpha^2 + N_{y0}\beta^2\right] + c_{2b}\left(w_{0mn}^2 + 2\xi h w_{0mn}\right)(w_{0mn} + \xi h) = 0 \tag{32}$$

where: $c_{1b} = \tilde{A}_{55}^s\alpha D_1 + \tilde{A}_{44}^s\beta D_2 + \frac{3}{4}K_w + \alpha^2\left(\tilde{A}_{55}^s + K_{sx}\right) + \beta^2\left(\tilde{A}_{44}^s + K_{sy}\right)$;

$$c_{2b} = D\left[\frac{5}{128}\left(\alpha^4 + \beta^4\right) - \frac{a^4\beta^4}{24\left(\alpha^2 + \beta^2\right)^2} + \frac{a^4\beta^4}{48\left(\alpha^2 + 4\beta^2\right)^2} + \frac{a^4\beta^4}{48\left(4\alpha^2 + \beta^2\right)^2}\right].$$

For an FGP plate subjected to bi-axial compressive loads $N_x^0 = -\gamma_1 N_0 h, N_y^0 = -\gamma_2 N_0 h$ in the sides $x = 0, a$ and $y = 0, b$, from the Eq. (32) we get:

$$N_0 = \frac{c_{1b}}{\gamma_1\alpha^2 + \gamma_2\beta^2}\frac{\bar{W}}{\left(\bar{W} + \xi\right)h} + \frac{c_{2b}}{\gamma_1\alpha^2 + \gamma_2\beta^2}\left(\bar{W}^2 + 2\xi\bar{W}\right)h \tag{33}$$

Similar to the SSSS boundary conditions, from Eq. (33) we can determine the relationship between compressive loads and deflection in case of perfect plates:

$$N_0^* = \frac{c_{1b}}{\left(\gamma_1\alpha^2 + \gamma_2\beta^2\right)h} + \frac{c_{2b}}{\gamma_1\alpha^2 + \gamma_2\beta^2}\bar{W}^2 h \tag{34}$$

and buckling loads:

$$N_{bl} = \frac{c_{1b}}{\left(\gamma_1\alpha^2 + \gamma_2\beta^2\right)h} \tag{35}$$

The buckling loads N_{bl} expressed by Eq. (35) belong to corresponding buckling modes (*m, n*). The critical buckling load N_{cr} is the minimal value of these buckling loads.

c. ***Boundary conditions SCSC***

For this case, the solutions are chosen as [27, 28]:

$$w_0 = w_{0mn} \sin \alpha x \sin^2 \beta y; \;\; \vartheta_x = \vartheta_{xmn} \cos \alpha x \sin^2 \beta y$$
$$\vartheta_y = \vartheta_{ymn} \sin \alpha x \sin 2\beta y; \;\; w_0^* = \xi h \sin \alpha x \sin^2 \beta y \tag{36}$$

Substituting Eq. (36) into Eq. (16), we have:

$$\nabla^4 \varphi = \frac{D\left(w_{0mn}^2 + 2\xi h w_{0mn}\right)\alpha^2 \beta^2}{2}(\cos 2\alpha x + \cos 2\beta y - \cos 4\beta y - \cos 2\alpha x \cos 2\beta y) \tag{37}$$

The stress function may be assumed in the following form:

$$\varphi = f_1 \cos 2\alpha x + f_2 \cos 2\beta y + f_3 \cos 4\beta y + f_4 \cos 2\alpha x \cos 2\beta y + N_{x0}\frac{y^2}{2} + N_{y0}\frac{x^2}{2} \tag{38}$$

where: $f_1 = \frac{D\beta^2}{32\alpha^2}\left(w_{0mn}^2 + 2\xi h w_{0mn}\right)$; $f_2 = \frac{D\alpha^2}{32\beta^2}\left(w_{0mn}^2 + 2\xi h w_{0mn}\right)$; $f_3 = -\frac{D\alpha^2}{512\beta^2}\left(w_{0mn}^2 + 2\xi h w_{0mn}\right)$; $f_4 = -\frac{D\alpha^2\beta^2}{32\left(\alpha^2+\beta^2\right)^2}\left(w_{0mn}^2 + 2\xi h w_{0mn}\right)$.

Putting Eq. (38) into Eqs. (13.2) and (13.3), applying Galerkin's procedure, we obtain rotations in term of deflections:

$$\vartheta_{xmn} = D_1 w_{0mn}; \;\; \vartheta_{ymn} = D_2 w_{0mn} \tag{39}$$

in which: $D_1 = \frac{B_1 C_2 - B_2 C_1}{A_1 B_2 - A_2 B_1}$; $D_2 = \frac{A_2 C_1 - A_1 C_2}{A_1 B_2 - A_2 B_1}$; $C_1 = 3\tilde{A}_{55}^s \alpha$; $C_2 = \tilde{A}_{44}^s \beta$; $A_1 = 3C_{11}\alpha^2 + 4C_{66}\beta^2 + 3A_{44}^s$; $A_2 = \left(\tilde{C}_{12} + \tilde{C}_{66}\right)\alpha\beta$; $B_1 = 4\left(\tilde{C}_{12} + \tilde{C}_{66}\right)\alpha\beta$; $B_2 = \tilde{C}_{66}\alpha^2 + 4\tilde{C}_{11}\beta^2 + \tilde{A}_{44}^s$.

By substituting Eqs. (38) and (39) into Eq. (13.1) and then implementing Galerkin's procedure, we get:

$$w_{0mn} c_{1c} + \left(3N_{x0}\alpha^2 + 4N_{y0}\beta^2\right)(w_{0mn} + \xi h) + c_{2c}\left(w_{0mn}^2 + 2\xi h w_{0mn}\right)(w_{0mn} + \xi h) = 0 \tag{40}$$

where: $c_{1c} = 3\tilde{A}_{44}^s \alpha D_1 + 4\tilde{A}_{44}^s \beta D_2 + 3K_w + 3\left(\tilde{A}_{44}^s + K_{sx}\right)\alpha^2 + 4\left(\tilde{A}_{44}^s + K_{sy}\right)\beta^2$;

$$c_{2c} = D\left[\frac{17\alpha^4}{64} + \frac{\beta^4}{4} + \frac{\alpha^4\beta^4}{8\left(\alpha^2 + \beta^2\right)^2}\right].$$

Similar to boundary conditions SSSS and CCCC, in case of boundary condition SCSC, the relationship between compressive loads and deflection is determined in case of imperfect plates subjected to bi-axial compressive loads $N_x^0 = -\gamma_1 N_0 h$, $N_y^0 = -\gamma_2 N_0 h$ at the edges $x = 0, a$ and $y = 0, b$:

$$N_0 = \frac{c_{1c}}{3\gamma_1\alpha^2 + 4\gamma_2\beta^2}\frac{\bar{W}}{\left(\bar{W} + \xi\right)h} + \frac{c_{2c}}{3\gamma_1\alpha^2 + 4\gamma_2\beta^2}\left(\bar{W}^2 + 2\xi\bar{W}\right)h. \tag{41}$$

For the perfect plate:

$$N_0^* = \frac{c_{1c}}{\left(3\gamma_1\alpha^2 + 4\gamma_2\beta^2\right)h} + \frac{c_{2c}}{3\gamma_1\alpha^2 + 4\gamma_2\beta^2}\bar{W}^2 h \tag{42}$$

From there, the buckling and critical loads are determined as follow:

$$N_{bl} = \frac{c_{1c}}{\left(3\gamma_1\alpha^2 + 4\gamma_2\beta^2\right)h} \quad \Rightarrow N_{cr} = \min\{N_{bl}\} \tag{43}$$

5 Numerical Results and Discussion

Based on the above mentioned presented analytical solution, the Matlab's code is built to implement numerical examples. Numerical results are presented for nonlinear analysis unless previously stated. For convenience, the nondimensional results are used in the form [29–31]:

$$\bar{N} = N_{cr}\frac{a^2}{E_1h^2};\ K_0 = \frac{K_w a^4}{E_0h^3};\ J_0 = \frac{K_{sx}a^2}{E_0h^3\nu} = \frac{K_{sy}b^2}{E_0h^3\nu};\ E_0 = 1.0\text{ GPa}; \tag{44}$$

5.1 Validation Examples

Example 1: Validation for isotropic plate.

Consider a simply supported isotropic rectangular plate ($e_0 = 0,\ h = 0.1\,in., a = 20\,in.,\ a/b = 2$) subjected to in-plane uniaxial compressive load (x-direction, $\gamma_1 = 1, \gamma_2 = 0$). Table 1 presents the critical loads $P_{cr} = bhN_{cr}$ of isotropic plates made of different materials such as Aluminum ($E = 10 \times 10^6\,psi,\ \nu = 0.3$), Titanium alloy ($E = 15.1 \times 10^6\,psi,\ \nu = 0.3$) and Stainless steel ($E = 30.1 \times 10^6\,psi,\ \nu = 0.3$). The obtained results are compared with those of Brush and Almroth [26] used the analytical method.

Table 1. Critical loads P_{cr} of simply supported isotropic rectangular plate under uniaxial compression in the x-direction ($\gamma_1 = 1, \gamma_2 = 0$)

P_{cr}[pound]	Brush and Almroth [26]	Present	Error (%)
$E = 10 \times 10^6\,psi,\ \nu = 0.3$ Aluminum (Al)	3620 (2, 1)[a]	3613.20 (2, 1)	0.188
$E = 15.1 \times 10^6\,psi,\ \nu = 0.3$ Titanium alloy (Ti-6Al-4V)	5459 (2, 1)	5455.93 (2, 1)	0.056
$E = 30.1 \times 10^6\,psi,\ \nu = 0.3$ Stainless steel (SUS304)	10882 (2, 1)	10875.74 (2, 1)	0.058

[a] *The numbers in brackets indicate the buckling mode (m, n)*

The post-buckling load-deflection curves N_{cr}/h- w_{0mn}/h of simply supported isotropic square plate ($e_0 = 0$, $E_1 = 380$ GPa, $\nu = 0.3$, $b/h = 40$) are illustrated in Fig. 3 for two cases: perfect plate ($\xi = 0$) and imperfect plate ($\xi = 0.1$). The results are compared with those given by Tung and Duc [16] using the classical plate theory.

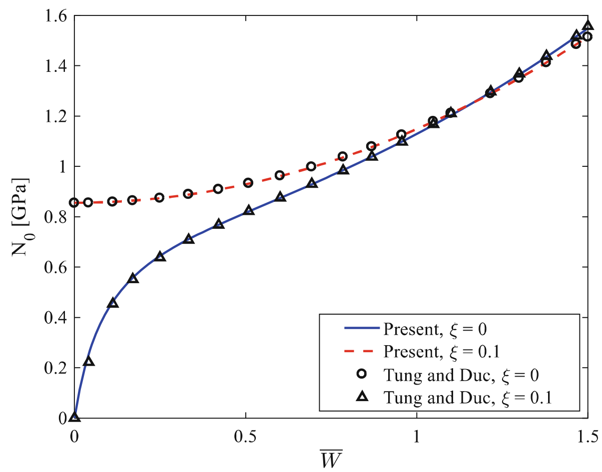

Fig. 3. Post-buckling load-deflection curves of the isotropic square plate

Table 2 presents the comparison of the nondimensional critical load $\hat{N} = \frac{hb^2}{C_{11}-B_{11}^2/A_{11}}N_{cr}$ of the isotropic square plate made of SiC ($E = 420$ GPa, $\nu = 0.3$, $a/h = 10$, $b/a = 1$, boundary conditions SSSS and SCSC) under bi-axial compressive loads ($\gamma_1 = \gamma_2 = 1$) with the results given by Thai và Choi [32] using analytical approach and refined four-variable shear deformation theory.

Table 2. Nondimensional critical loads P_{cr} of simply supported isotropic rectangular plate subjected to bi-axial compressive loads ($\gamma_1 = \gamma_2 = 1$)

Method	SSSS	SCSC
Thai and Choi [32]	18.6861	34.1195
Present	18.6854	33.9600
Error (%)	0.004	0.467

Example 1: Validation for functionally graded porous plate.
Table 3 shows the values of nondimensional critical load of square FGP plates under uniaxial in-plane compression in x-direction ($a/h = 10$, $b/a = 1$, $\gamma_1 = 1$, $\gamma_2 = 0$) with different porosity coefficients e_0 and two porosity distribution patterns: uniform and non-uniform symmetric. The porous plate made of metal foam with material properties: $G_1 = 26, 293$ GPa, $\nu = 0.3$, $E_1 = 2G_1(1 + \nu)$ [10]. The obtained results are compared with those of Thang et al. [31] using Navier's solution and FSDT.

From two above-mentioned validation examples, a good agreement can be found.

Table 3. Nondimensional critical loads $\bar{N} = N_{cr}a^2/E_1h^2$ of simply supported FGP plate under uniaxial in-plane compression ($\gamma_1 = 1,\ \gamma_2 = 0,\ b/a = 1,\ a/h = 10$)

Porosity distribution	Sources	e_0					
		0.1	0.2	0.3	0.4	0.5	0.6
Uniform	Thang et al. [31]	3.2109	2.9856	2.7549	2.5173	2.2710	2.0135
	Present	3.2023	2.9777	2.7475	2.5105	2.2650	2.0081
	Error (%)	0.268	0.265	0.269	0.270	0.264	0.268
Non-uniform symmetric	Thang et al. [31]	3.3023	3.1729	3.0432	2.9130	2.7822	2.6506
	Present	3.2933	3.1640	3.0343	2.9041	2.7733	2.6417
	Error (%)	0.273	0.281	0.292	0.306	0.320	0.336

5.2 Parametric Study

In this section, the effect of material properties, boundary conditions, elastic foundation parameters, and initial imperfection on buckling and post-buckling response of FGP plates is examined.

Consider the metal foam rectangular plate resting in Pasternak's elastic foundation with input data: $h = 0.1$ m, $E_1 = 200$ GPa, $\nu = 1/3$. This plate subjected to bi-axial in-plane compression $N_x^0 = -\gamma_1 N_0 h$, $N_y^0 = -\gamma_2 N_0 h$ at the edges $x = 0, a$ and $y = 0, b$.

Table 4 presents nondimenssional critical loads $\bar{N}$ and corresponding buckling modes of perfect square FGP plates ($h = 0.1$ m, $b/a = 1$, $a/h = 10$; $K_0 = J_0 = 0$) with three porosity distribution patterns namely Type 1 (uniform), Type 2 (symmetric), and Type 3 (non-symmetric), and different porosity coefficients ($e_0 = 0.1$; 0.3; 0.5 and 0.8). The plate under various BCs: SSSS, CCCC and SCSC, and subjected to uniaxial in-plane compression.

Table 4. Nondimensional critical loads $\bar{N}$ of square FGP plates with different porosity coefficients e_0 and various porosity distribution patterns under three boundary condition types

Boundary condition	Porosity distribution types	e_0			
		0.1	0.3	0.5	0.8
SSSS, $\gamma_1 = 1, \gamma_2 = 0$	Type 1 (uniform)	$3.2696^{(1,1)}$	$2.8053^{(1,1)}$	$2.3126^{(1,1)}$	$1.4676^{(1,1)}$
	Type 2 (symmetric)	$3.3623^{(1,1)}$	$3.0973^{(1,1)}$	$2.8302^{(1,1)}$	$2.4222^{(1,1)}$
	Type 3 (non-symmetric)	$3.2869^{(1,1)}$	$2.8486^{(1,1)}$	$2.3639^{(1,1)}$	$1.4688^{(1,1)}$
CCCC, $\gamma_1 = 1, \gamma_2 = 0$	Type 1 (uniform)	$7.9758^{(1,1)}$	$6.8431^{(1,1)}$	$5.6413^{(1,1)}$	$3.5800^{(1,1)}$
	Type 2 (symmetric)	$8.1825^{(1,1)}$	$7.4943^{(1,1)}$	$6.7949^{(1,1)}$	$5.7078^{(1,1)}$
	Type 3 (non-symmetric)	$8.0148^{(1,1)}$	$6.9442^{(1,1)}$	$5.7701^{(1,1)}$	$3.6273^{(1,1)}$

(*continued*)

Table 4. (*continued*)

Boundary condition	Porosity distribution types	e_0			
		0.1	0.3	0.5	0.8
SCSC, $\gamma_1 = 1, \gamma_2 = 0$	Type 1 (uniform)	$5.8520^{(2,1)}$	$5.0209^{(2,1)}$	$4.1391^{(2,1)}$	$2.6267^{(2,1)}$
	Type 2 (symmetric)	$6.0004^{(2,1)}$	$5.4887^{(2,1)}$	$4.9679^{(2,1)}$	$4.1562^{(2,1)}$
	Type 3 (non-symmetric)	$5.8801^{(2,1)}$	$5.0943^{(2,1)}$	$4.2343^{(2,1)}$	$2.6689^{(2,1)}$
SCSC, $\gamma_1 = 0, \gamma_2 = 1$	Type 1 (uniform)	$5.1855^{(1,1)}$	$4.4491^{(1,1)}$	$3.6678^{(1,1)}$	$2.3276^{(1,1)}$
	Type 2 (symmetric)	$5.3237^{(1,1)}$	$4.8844^{(1,1)}$	$4.4389^{(1,1)}$	$3.7496^{(1,1)}$
	Type 3 (non-symmetric)	$5.2115^{(1,1)}$	$4.5157^{(1,1)}$	$3.7508^{(1,1)}$	$2.3496^{(1,1)}$

[a] *The number in brackets indicate the buckling mode (m, n)*

The variation of nondimensional critical loads with respect to porosity coefficients and various porosity distribution patterns is illustrated in Fig. 4: (a) SSSS, $\gamma_1 = 1, \gamma_2 = 0$; (b) CCCC, $\gamma_1 = 1, \gamma_2 = 0$; (c) SCSC, $\gamma_1 = 1, \gamma_2 = 0$; (d) SCSC, $\gamma_1 = 0, \gamma_2 = 1$. The obtained results indicated that when porosity coefficients increase, the critical buckling

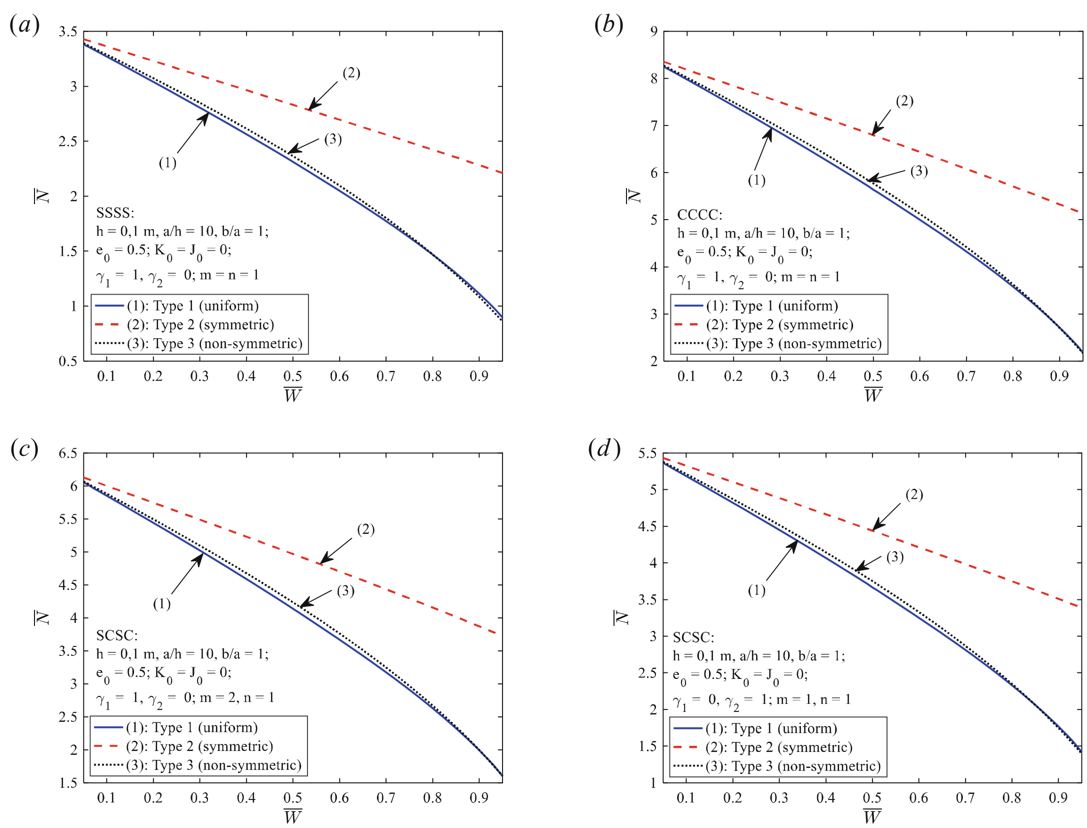

Fig. 4. The variation of nondimensional critical loads of square FGP plates with respect to porosity coefficients e_0 and porosity distribution patterns: (a) SSSS, $\gamma_1 = 1, \gamma_2 = 0$; (b) CCCC, $\gamma_1 = 1, \gamma_2 = 0$; (c) SCSC, $\gamma_1 = 1, \gamma_2 = 0$; (d) SCSC, $\gamma_1 = 0, \gamma_2 = 1$

loads of FGP plates decrease for all patterns of porosity distribution. This is due to an increase in the porosity coefficient that results in a reduction of FGP plate stiffness. The critical buckling loads of Type 2 (non-uniform symmetric) are the highest. The critical buckling loads of Type 1 (uniform) and Type 3 (non-uniform symmetric) distributions are slightly different.

The effect of boundary conditions is clearly illustrated: as expected, the critical buckling load of the CCCC plate is the highest and of the SSSS plate is the smallest.

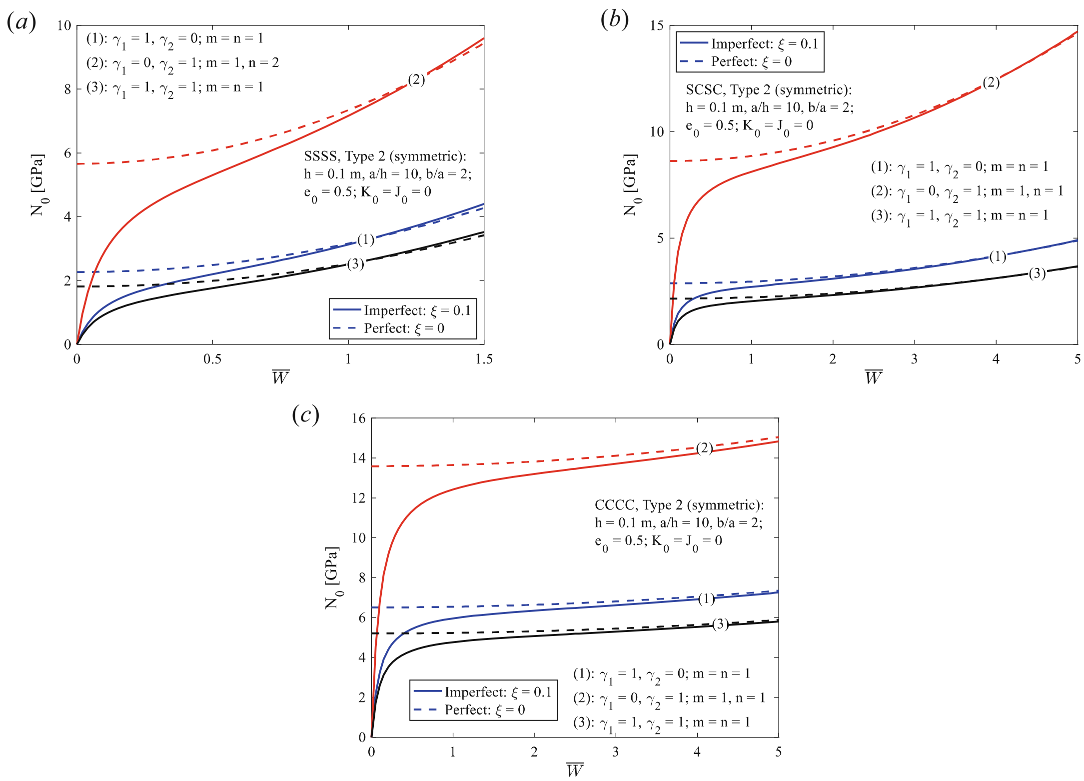

Fig. 5. The effect of in-plane compressive load types on the post-buckling load-deflection curves for the SSSS (a), SCSC (b) and CCCC (c) FGP plates

Figure 5 shows post-buckling load-deflection curves of perfect and imperfect rectangular FGP ($h = 0.1$m, $a/h = 10$, $b/a = 2$, $e_0 = 0.5$, $K_0 = J_0 = 0$) with Type 2 porosity distribution under different types of in-plane compressive loads. As can be observed that the post-buckling curve of the bi-axial compressive load is the lowest, and the curve of uniaxial compressive loads along the shorter edge is the highest for all cases of boundary conditions. Besides, it is seen that better resistance to compression in the longer side than the shorter side.

Effect of porosity distribution and porosity coefficient on the post-buckling load-deflection curves of perfect and imperfect simply supported (SSSS) rectangular FGP plates ($h = 0.1$m, $a/h = 10$, $b/a = 2$, $e_0 = 0.5$, $K_0 = J_0 = 0$) under uniaxial compression (x-direction) is shown in Fig. 6 and 7. It can be seen that the post-buckling load-deflection curves for Type 2 distribution are higher than remain two distribution types; the higher porosity coefficient, the lower post-buckling load-deflection curve. This trend is similar for both perfect and imperfect plates.

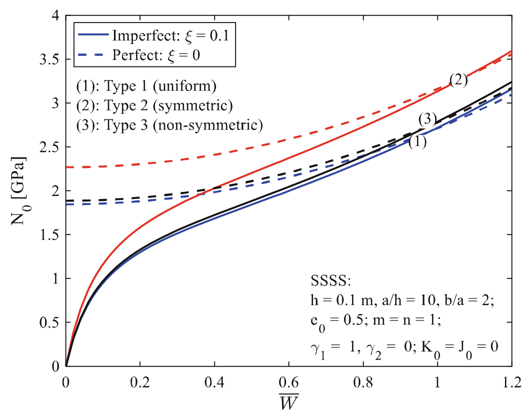

Fig. 6. Effect of porosity distribution patterns on post-buckling of FGP plates

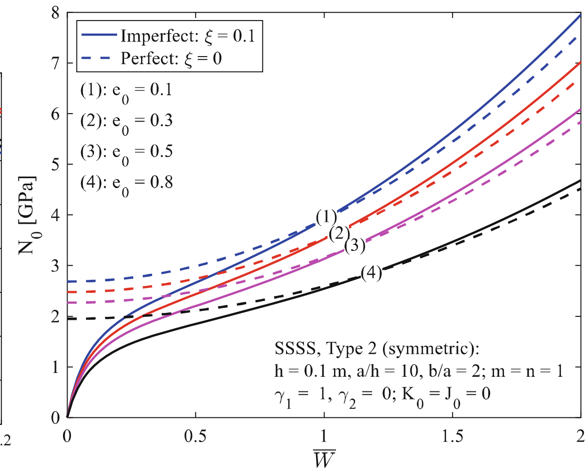

Fig. 7. Effect of porosity coefficients e_0 on post-buckling of FGP plates

Figure 8 shows the influence of imperfection size on the post-buckling response of simply supported FGP plates ($h = 0.1$ m, $a/h = 10$, $b/a = 2$, $K_0 = J_0 = 0$,) under uniaxial (x-direction) compression. It is obvious that the post-buckling curves of perfect FGP plates are higher than those of imperfect FGP plates when deflection is small.

The effect of Winkler and Pasternak elastic foundation stiffness on load-deflection curves of simply supported FGP plates ($h = 0.1$m, $a/h = 10$, $b/a = 2$, $e_0 = 0.5$) under uniaxial (x-direction) compression is depicted in Fig. 9. It figure shows that the post-buckling load-deflection curves become higher as the linear Winkler foundation parameter K_0 and Pasternak foundation parameter J_0 increased. Furthermore, the effect of Pasternak foundation is larger than the Winkler foundation.

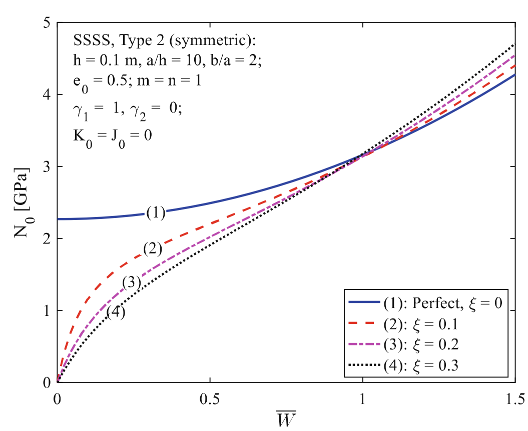

Fig. 8. The effect of the imperfection ξ on the post-buckling of FGP plates

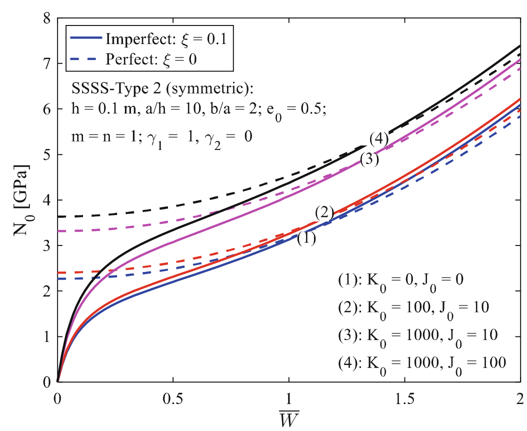

Fig. 9. The effect of elastic foundation parameters on the post-buckling of FGP plates

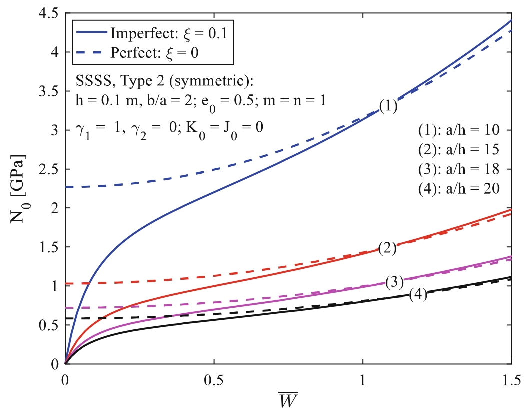

Fig. 10. The effect of the side-to-thickness ratio a/h on post-buckling of FGP plates

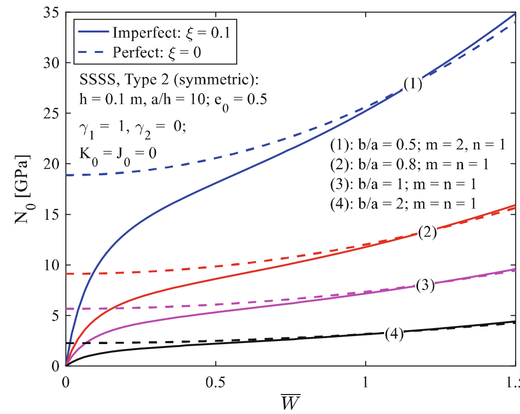

Fig. 11. The effect of aspect ratio b/a on post-buckling of FGP plate

The Figs. 10 and 11 depict the effect of side-to-thickness ratio *a/h* and aspect ratio *b/a* on the post-buckling behavior of perfect and imperfect simply supported rectangular FGP plates ($h = 0.1$ m, $e_0 = 0.5$, $K_0 = J_0 = 0$) with Type 2 porosity distribution, respectively. It can be seen that the post-buckling load-deflection curves of imperfect ($\xi = 0.1$) and perfect ($\xi = 0$) plates move downward as the side-to-thickness ratio *a/h* and aspect ratio *b/a* increase. In other words, when the side-to-thickness ratio *a/h* and aspect ratio *b/a* increase, the bearing load capacity decreases.

6 Conclusions

In this paper, the buckling and post-buckling analysis of FGP plates resting on Pasternak elastic foundation and subjected to in-plane compressive loads are presented based on the first-order shear deformation theory. The initial geometrical imperfection is taken into account. Three porosity distribution patterns namely uniform, non-uniform symmetric, non-uniform asymmetric are considered. By using the Galerkin method and Airy's stress function, the analytical solution is developed for FGP rectangular plates under various types of boundary condition.

The validate examples are conducted and the accuracy between obtained results and published ones is found. Numerical results indicate the significant effects of material parameters (porosity coefficient, porosity distribution patterns), geometric parameters (aspect and side-to-thickness ratio), initial geometrical imperfection, elastic foundation as well as in-plane boundary conditions on the critical buckling loads and the post-buckling response of FGP plates.

Acknowledgements. This research is funded by the Ministry of Education and Training for Science and Technology Project under grant number: CT.2019.03.04.

References

1. Smith, B.H., Szyniszewski, S., Hajjar, J.F., Schafer, B.W., Arwade, S.R.: Steel foam for structures: a review of applications, manufacturing and material properties. J. Constr. Steel Res. **71**, 1–10 (2012)
2. Ashby, M.F., et al.: Metal foams: a design guide. Appl. Mech. Rev. **54**(6), B105–B106 (2001)
3. Lefebvre, L.P., Banhart, J., Dunand, D.C.: Porous metals and metallic foams: current status and recent developments. Adv. Eng. Mater. **10**(9), 775–787 (2008)
4. Wattanasakulpong, N., Ungbhakorn, V.: Linear and nonlinear vibration analysis of elastically restrained ends FGM beams with porosities. Aerosp. Sci. Technol. **32**(1), 111–120 (2014)
5. Chen, D., Yang, J., Kitipornchai, S.: Elastic buckling and static bending of shear deformable functionally graded porous beam. Compos. Struct. **133**, 54–61 (2015)
6. Chen, D., Yang, J., Kitipornchai, S.: Free and forced vibrations of shear deformable functionally graded porous beams. Int. J. Mech. Sci. **108**, 14–22 (2016)
7. Chen, D., Kitipornchai, S., Yang, J.: Nonlinear free vibration of shear deformable sandwich beam with a functionally graded porous core. Thin-Walled Struct. **107**, 39–48 (2016)
8. Jabbari, M., Mojahedin, A., Khorshidvand, A.R., Eslami, M.R.: Buckling analysis of a functionally graded thin circular plate made of saturated porous materials. J. Eng. Mech. **140**(2), 287–295 (2014)
9. Jabbari, M., Hashemitaheri, M., Mojahedin, A., Eslami, M.R.: Thermal buckling analysis of functionally graded thin circular plate made of saturated porous materials. J. Therm. Stresses **37**(2), 202–220 (2014)
10. Rezaei, A.S., Saidi, A.R.: Application of Carrera Unified Formulation to study the effect of porosity on natural frequencies of thick porous–cellular plates. Compos. Part B Eng. **91**, 361–370 (2016)
11. Rezaei, A.S., Saidi, A.R., Abrishamdari, M., Mohammadi, M.P.: Natural frequencies of functionally graded plates with porosities via a simple four variable plate theory: an analytical approach. Thin-Walled Struct. **120**, 366–377 (2017)
12. Akbaş, ŞD.: Vibration and static analysis of functionally graded porous plates. J. Appl. Comput. Mech. **3**(3), 199–207 (2017)
13. Liew, K.M., Yang, J., Kitipornchai, S.: Postbuckling of piezoelectric FGM plates subject to thermo-electro-mechanical loading. Int. J. Solids Struct. **40**(15), 3869–3892 (2003)
14. Bakora, A., Tounsi, A.: Thermo-mechanical post-buckling behavior of thick functionally graded plates resting on elastic foundations. Struct. Eng. Mech. **56**(1), 85–106 (2015)
15. Feyzi, M.R., Khorshidvand, A.R.: Axisymmetric post-buckling behavior of saturated porous circular plates. Thin-Walled Struct. **112**, 149–158 (2017)
16. Van Tung, H., Duc, N.D.: Nonlinear analysis of stability for functionally graded plates under mechanical and thermal loads. Compos. Struct. **92**(5), 1184–1191 (2010)
17. Cong, P.H., Chien, T.M., Khoa, N.D., Duc, N.D.: Nonlinear thermomechanical buckling and post-buckling response of porous FGM plates using Reddy's HSDT. Aerosp. Sci. Technol. **77**, 419–428 (2018)
18. Barati, M.R., Zenkour, A.M.: Analysis of postbuckling behavior of general higher-order functionally graded nanoplates with geometrical imperfection considering porosity distributions. Mech. Adv. Mater. Struct. **26**(12), 1081–1088 (2019)
19. Phung-Van, P., Thai, C.H., Ferreira, A.J.M., Rabczuk, T.: Isogeometric nonlinear transient analysis of porous FGM plates subjected to hygro-thermo-mechanical loads. Thin-Walled Struct. **148,** 106497 (2020)
20. Tu, T.M., Hoa, L.K., Hung, D.X., Hai, L.T.: Nonlinear buckling and post-buckling analysis of imperfect porous plates under mechanical loads. J. Sandwich Struct. Mater. **22**(6), 1910–1930 (2020)

21. Binh, C.T., Van Long, N., Tu, T.M., Minh, P.Q.: Nonlinear vibration of functionally graded porous variable thickness toroidal shell segments surrounded by elastic medium including the thermal effect. Compos. Struct. **255**, 112891 (2020)
22. Barati, M.R., Zenkour, A.M.: Investigating post-buckling of geometrically imperfect metal foam nanobeams with symmetric and asymmetric porosity distributions. Compos. Struct. **182**, 91–98 (2017)
23. Larbi, L.O., Kaci, A., Houari, M.S.A., Tounsi, A.: An efficient shear deformation beam theory based on neutral surface position for bending and free vibration of functionally graded beams#. Mech. Based Des. Struct. Mach. **41**(4), 421–433 (2013)
24. Reddy, J.N.: Theory and Analysis of Elastic Plates and Shells. CRC Press, Boca Raton (2006)
25. Reddy, J.N.: Energy Principles and Variational Methods in Applied Mechanics. Wiley, Hoboken (2017)
26. Brush, D.O., Almroth, B.O.: Buckling of Bars, Plates, and Shells. Mc GrawHill, New York (1975)
27. Sobhy, M.: Buckling and free vibration of exponentially graded sandwich plates resting on elastic foundations under various boundary conditions. Compos. Struct. **99**, 76–87 (2013)
28. Meziane, M.A.A., Abdelaziz, H.H., Tounsi, A.: An efficient and simple refined theory for buckling and free vibration of exponentially graded sandwich plates under various boundary conditions. J. Sandwich Struct. Mater. **16**(3), 293–318 (2014)
29. Thai, H.T., Choi, D.H.: A refined plate theory for functionally graded plates resting on elastic foundation. Compos. Sci. Technol. **71**(16), 1850–1858 (2011)
30. Zenkour, A.M.: The refined sinusoidal theory for FGM plates on elastic foundations. Int. J. Mech. Sci. **51**(11–12), 869–880 (2009)
31. Thang, P.T., Nguyen-Thoi, T., Lee, D., Kang, J., Lee, J.: Elastic buckling and free vibration analyses of porous-cellular plates with uniform and non-uniform porosity distributions. Aerosp. Sci. Technol. **79,** 278–287 (2018)
32. Thai, H.T., Choi, D.H.: An efficient and simple refined theory for buckling analysis of functionally graded plates. Appl. Math. Model. **36**(3), 1008–1022 (2012)